






Article

Analyzing the Impact of Urban Planning and Building Typologies in Urban Heat Island Mitigation

Dionysia Kolokotsa ^{1,*}, Katerina Lilli ¹, Kostas Gobakis ¹, Angeliki Mavrigiannaki ¹, Shamila Haddad ², Samira Garshasbi ², Hamed Reza Heshmat Mohajer ², Riccardo Paolini ², Konstantina Vasilakopoulou ², Carlos Bartesaghi ³, Deo Prasad ² and Mattheos Santamouris ²

- ¹ Chemical and Environmental Engineering School, Technical University of Crete Kounoupidiana, GR 73100 Chania, Crete, Greece; alilli@isc.tuc.gr (K.L.); kgobakis@isc.tuc.gr (K.G.); amavrigiannaki@isc.tuc.gr (A.M.)
- ² School of Built Environment, UNSW, Sydney, NSW 2052, Australia; s.haddad@unsw.edu.au (S.H.); s.garshasbi@unsw.edu.au (S.G.); h.heshmatmohajer@unsw.edu.au (H.R.H.M.); r.paolini@unsw.edu.au (R.P.); k.vasilakopoulou@unsw.edu.au (K.V.); d.prasad@unsw.edu.au (D.P.); m.santamouris@unsw.edu.au (M.S.)
- ³ School of Architecture and Built Environment, The University of Adelaide, Adelaide, SA 5005, Australia; carlos.bartesaghi@adelaide.edu.au
- * Correspondence: dkolokotsa@chenverg.tuc.gr

Abstract: Urban and building typologies have a serious impact on the urban climate and determine at large the magnitude of the urban overheating and urban heat island intensity. The present study aims to analyze the impact of various city typologies and urban planning characteristics on the mitigation of the urban heat island. The effect of the building height, street width, aspect ratio, built area ratio, orientation, and dimensions of open spaces on the distribution of the ambient and surface temperature in open spaces is analyzed using the Sydney Metropolitan Area as a case study for both unmitigated and mitigated scenarios. Fourteen precincts are developed and simulated using ENVI-met the simulation tool. The ambient temperature, surface temperature, and wind speed are extracted. The parameter ‘Gradient of the Temperature Decrease along the Precinct Axis’ (GTD) is introduced to study the cooling potential of the various precincts. In the mitigated precincts, the GTD ranges between 0.01 K/m to 0.004 K/m. In the non-mitigated precincts, the GTD ranges between 0.0093 K/m to 0.0024 K/m. A strong correlation is observed between the GTD of all the precincts, with and without mitigation, and their corresponding average aspect ratio, (Height of buildings to Width of streets). The higher the aspect ratio of the precinct, the lower the cooling potential. It is also observed that the higher the Built Area Ratio of the precincts, the lower the cooling contribution of the mitigation measures.

Keywords: urban climate; urban heat island; urban heat island mitigation; cool materials; urban green



Citation: Kolokotsa, D.; Lilli, K.; Gobakis, K.; Mavrigiannaki, A.; Haddad, S.; Garshasbi, S.; Mohajer, H.R.H.; Paolini, R.; Vasilakopoulou, K.; Bartesaghi, C.; et al. Analyzing the Impact of Urban Planning and Building Typologies in Urban Heat Island Mitigation. *Buildings* **2022**, *12*, 537. <https://doi.org/10.3390/buildings12050537>

Academic Editor: Wahidul K. Biswas

Received: 8 February 2022

Accepted: 12 April 2022

Published: 23 April 2022

Publisher’s Note: MDPI stays neutral with regard to jurisdictional claims in published maps and institutional affiliations.



Copyright: © 2022 by the authors. Licensee MDPI, Basel, Switzerland. This article is an open access article distributed under the terms and conditions of the Creative Commons Attribution (CC BY) license (<https://creativecommons.org/licenses/by/4.0/>).

1. Introduction

The heat island effect is the most documented phenomenon of climate change. The phenomenon has been known for almost a century and is related to higher urban temperatures compared to the adjacent suburban and rural areas. Higher urban temperatures are due to the positive thermal balance of urban areas caused by several factors such as [1–5]:

- The release of anthropogenic heat;
- The excess storage of solar radiation by the city structures;
- The lack of green spaces and cool sinks;
- The non-circulation of air in urban canyons;
- The reduced ability of the emitted infrared radiation to escape in the atmosphere.

Summer urban heat islands with daytime average air temperatures 4 °C higher than the surrounding rural areas are present in many cities around the world.

Urban overheating has a serious impact on the energy consumption of buildings and the peak electricity demand, while it increases the concentration of urban pollutants and seriously affects the levels of heat-related mortality and morbidity, [6–9].

In Sydney, the phenomenon has been studied in depth [10–13] with a maximum recorded gradient of peak temperature of 9 °C. Such a high magnitude of the urban heat island is due to the existence of two synoptic meteorological systems affecting the local climate. In particular, sea breeze contributes to lower ambient temperature in the eastern coastal part of the city, while warm western winds from the desert heat the western part of the city, [14,15].

To counterbalance the impact of urban overheating, important heat mitigation technologies and techniques have been developed [16–18]. Mitigation technologies aim to decrease the maximum possible heat gains and maximize the heat losses in a city to decrease the magnitude of the urban overheating. The increase of the urban albedo as well as the use of additional greenery (green roofs, walls, green parks, pocket parks, etc.) [19–21], evaporative sources, blue infrastructure [22,23] low-temperature heat sinks seems to be among the most efficient ones [24–27].

Urban and building typologies have a serious impact on the urban climate and determine at large the magnitude of the urban overheating [13,28,29]. The urban density, height of buildings, size of streets, aspect ratio, and size of open spaces affect the heat and solar gain while determining the heat losses through radiation and convection [30,31]. While numerous studies are available on the impact of the various mitigation technologies, i.e., an increase of urban albedo and greenery, evaporative sources, etc., on urban climate, very little is known about the heat impact of the main landscape parameters as well as their impact on the cooling potential of the main mitigation technologies [32,33]. Therefore, although the impact of the various mitigation techniques on the urban heat island has been studied, the role of the spatial distribution, typologies, and urban forms play a significant role in the cooling potential of the various technologies. The present study aims to analyze the impact of building height, street width, aspect ratio, built area ratio, orientation, and dimensions of open spaces on the distribution of the ambient and surface temperature as well as on thermal comfort in open spaces. Moreover, the study analyses the impact of cooling potential of the most commonly used urban heat island mitigation technologies. The overall study is based on real urban neighborhoods with significant overheating problems.

The paper is structured in six more sections. Section 2 includes the methodology and approach of the research while Section 3 includes the description of the urban context in Sydney. The modeling procedures and simulation results are included in Sections 4 and 5 respectively while the analysis of results and conclusions are incorporated in Sections 6 and 7.

2. Materials and Methods

The present study aims to analyze the impact of various city typologies and urban planning characteristics on the mitigation of the urban heat island. For that purpose, Sydney Metropolitan Area is selected as the case study area for the following reasons:

- The neighborhoods represent real case areas.
- There is a good representation of open and compact typologies defined officially by the Australian Association of Planners.

There is a 100% representation of the specific urban area characteristics.

Sydney's climatic conditions are humid subtropical (Köppen: Cfa) in Eastern Australia [34]. In the Sydney Metropolitan Area (SMA), seven urban areas with diverse urban fabric characteristics are selected (see Tables 1 and 2). The residential areas have been categorized into 14 residential precincts to support microclimatic analysis. The Local Climate Zones (LCZs) approach has been followed for selecting the typologies. The LCZs is a standardized approach, widely implemented for the analysis of urban areas' overheating [35].

Table 1. Building Types.






Type	Description	Figure	No of Storeys	People per Hectare	Location	Amenities
T1: Single Dwellings	Single dwellings areas include houses, terrace houses, dual occupancies, and semi-detached dwellings.		1–2	30–100	Suburban areas	Local parks, distant shops
T2: Low Rise	Low rise housing typically involves townhouses/terrace housing or small-scale buildings with street-level retail shops and cafes with residential apartments above.		3–4	70–200	Close to village centers, along transport corridors	Parks, shops
T3: Low/Medium Rise	Low/medium-rise housing involves apartment buildings sometimes with cafes or small shops at the ground level.		5–6	150–300	Close to town centers and urban renewal areas	Park, shops, swimming pools
T4: Medium Rise	Medium rise housing involves apartment buildings, sometimes with cafes or medium shops at the ground level.		7–8	250–400	Urban corridors, urban renewal areas, city centers	Parks, shops, gyms, child cares, swimming pools, buses, trains
T5: Medium/High Rise	Medium /high-rise housing involves apartment buildings, sometimes with retail, medium, and large shops at the ground level.		9–12	300–400	Urban corridors, urban renewal areas, near railway stations	Parks, supermarket, gyms, child cares, swimming pools, buses, trains, theatres/cinemas

Table 1. Cont.

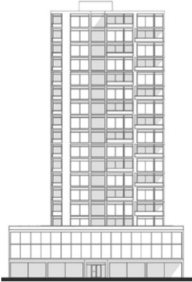
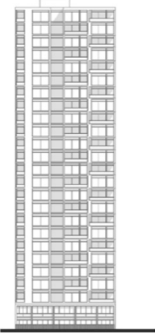
Type	Description	Figure	No of Storeys	People per Hectare	Location	Amenities
T6: High Rise 1	High rise housing 1 comprises standalone apartment buildings and mixed-use buildings that incorporate retail shops and/or commercial uses on the lower levels.		13–25	400–800	Near transport nodes, urban renewal areas, city centers	Parks, jobs, supermarkets, gyms, child cares, swimming pools, buses, trains, theatres/cinemas
T7: High Rise 2	High rise housing 1 comprises standalone residential and mixed-use towers that incorporate retail shops and/or commercial uses on the lower levels.		25+	600–1200	City centers, near railway stations	Parks, jobs, supermarkets, gyms, clubs, swimming pools, buses, theatres/cinemas, major railway st.

Table 2. District Precincts.










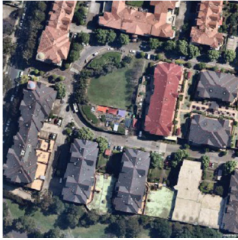




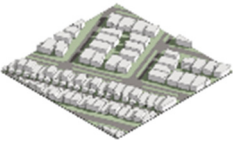











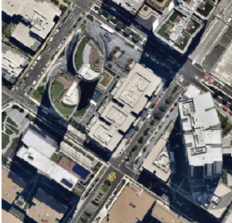
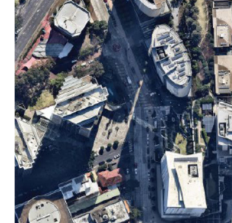
		Open Arrangements						
Type	OT1: Open Single Dwellings	OT2: Open Low Rise	OT3: Open Low/Medium Rise	OT4: Open Medium Rise	OT5: Open Medium/High Rise	OT6: Open High Rise 1	OT7: Open High Rise 2	
Figure								
Region in Sydney								
Location	Normanhurst	Kooloora	Rosebery	Raleigh Park	Parramatta	Waterloo	Sydney Olympic Park	
No. Storeys	1	3	5–6	8	9–12	18	30–35	
Building height	4–8	5–12	9–18	25–30	21–42	60	100–130	
Street width	25–35	25–30	15–20	35–45	20–30	45–55	30–70	
Building size	200–350	250–500	1000–2000	1000–1500	1000–1500	1000	1000–1500	

Table 2. Cont.

Compact arrangements							
Type	CT1: Compact single dwellings	CT2: Compact Low rise	CT3: Compact Low/Medium Rise	CT4: Compact Medium rise	CT5: Compact Medium/high rise	CT6: Compact High rise 1	CT7: Compact High rise 2
Figure							
Region in Sydney							
Location	Kellyville	Epping	Meadowback	Harold Park	Mascot	Wentworth Point	Chatswood
No. Storeys	1–2	3–4	6	7–8	10–12	15–25	35–40
Building height	4–12	8–12	12–18	21–30	28–42	60–75	130–145
Street width	25–30	15–30	15–20	20–25	25–30	25–30	25–40
Building size	150–300	650–1000	1000–2000	1000–1500	4000–6000	1500–2000	1000–1500

Seven residential building types (T1-T7, Table 1) have also been selected, representative of the area under investigation in this study. The building types are categorized according to height based on the typologies defined by the Department of Planning and Environment in New South Wales (NSW).

The seven building types are arranged under two urban design scenarios including one low density-open scenario (open represented by the letter 'O') and one high density-compact scenario (compact represented by the letter 'C'). Therefore 14 precincts are investigated corresponding to OT1-OT7 and CT1-CT7.

Current climate and land use as well as future climate and land use in 2050 have been simulated with mesoscale models. In addition, microscale climatic simulations for all the climatic scenarios are performed with hourly climatic files [36].

Microscale simulations are performed to predict the distribution of ambient temperature, wind speed, surface temperature, and outdoor thermal comfort, in the 14 precincts. The simulations are run for representative summer days based on the 2050 climate scenario. Two scenarios are simulated: (a) Full mitigation scenario, including implementation of greenery, evaporation, and cool materials in all precincts, and (b) Non-mitigation scenario where no mitigation measures are implemented.

The simulation results of the peak daytime temperature conditions are analyzed for assessing the distribution of the main climatic parameters and the outdoor thermal comfort. Moreover, the urban typologies characteristics are analyzed versus their cooling potential

The methodological steps are the following:

1. The building typologies and urban precincts are selected to fully represent the urban characteristics and neighborhoods.
2. The precincts are modeled using ENVI-met for the mitigated and unmitigated scenarios.
3. The ambient temperature, surface temperature, outdoor comfort indices, and wind flow regimes for both mitigated and unmitigated scenarios are extracted and compared.
4. The cooling potential is then analyzed by introducing a specific parameter called 'Gradient of the Temperature Decrease along the Precinct Axis' (GTD).
5. The GTD is evaluated versus the flow through open areas, the aspect ration (H/W), and the Built Area Ratio.

3. Buildings and Urban Context

Most urban precincts are not completely homogenous, and the different regions are composed of buildings with varying heights arranged in distinct patterns and densities thus providing various open spaces' typologies. Accordingly, the seven building typologies (Table 1) are further categorized into two arrangement types (open and compact) as mentioned in the previous section. The residential precincts are presented in Table 2. The further separation is based on four basic characteristics (no. stories, building height, street width, and building size).

4. Modeling Procedures

The simulations of the unmitigated and mitigated scenarios based on future climate (2050) were performed with the software ENVI-met V4.4.2 [37,38]. This program is a reliable tool for the simulation of the main climatic parameters' distribution in the urban environment. The program uses a three-dimensional microclimate model with a resolution that allows for simulating the surface, plant, and air interactions in urban environments. It supports microscale modeling with the following characteristics:

- A typical horizontal resolution from 0.5 to 5 m
- A typical time frame of 24 to 48 h
- A time step of 1 to 5 s.

ENVI-met solves the Reynolds-averaged non-hydrostatic Navier-Stokes equations for each grid in space and for each time step.

The spatial resolution used in the simulations of the present study is 1.5 m horizontally. The area has been represented with $150 \times 150 \times 30$ (x - y - z) cells. Each cell size is

$dx = 1.5$ m, $dy = 1.5$ m, and base $dz = 0.5$ m. The grid at the z-axis is telescopic with a thicker cell near the ground, allowing a better accuracy for edge effects.

Future climate conditions for 2050 are predicted with mesoscale models using the Weather Research and Forecasting (WRF) Model. The outputs of the mesoscale models are used as inputs to the ENVI-met microscale models.

For the ENVI-met simulations, two approaches are used: full forcing and simple forcing. Full forcing is used for the simulation of air temperature, relative humidity, and solar radiation. This means that the diurnal variation of the atmospheric boundary conditions and the incoming radiation is defined in each simulation step. The initial conditions for wind speed and direction are:

1. Wind speed: 2.5 m/s;
2. Wind direction: 250°;
3. The start time and date of simulation: 18:00 21/2/2050;
4. The end time and date of simulation: 00:00 23/2/2050 correspond to summer conditions in Sydney.

The buildings' characteristics are tabulated in Table 3 while the buildings' materials properties are tabulated in Tables 4 and 5. The vegetation types are included in Table 6 and the ENV-met models in Table 7.

Table 3. The buildings' construction characteristics.

Code	Name	Construction		
		Outside Layer	1st Layer	2nd Layer
000000	Default wall-moderate insulation	0100PL (1cm)	0100IN (11 cm)	0100CO (6 cm)
0100Q2	CoolRoof-moderate insulation	0100Q1 (1 cm)	0100FE (11 cm)	0100F3 (6 cm)

Table 4. The building materials' properties are used for all typologies.

Code	Name	Absorption	Reflection	Emissivity	Specific Heat (J/(kgK))	Thermal Conductivity (w/(mK))	Density (kg/m ³)
0100PL	Default Plaster	0.50	0.50	0.90	850	0.60	1500
0100Q1	CoolPaint	0.30	0.70	0.90	830	0.84	1856
0100IN	Default Insulation	0.50	0.50	0.90	1500	0.07	400
0100CO	Default Concrete	0.50	0.50	0.90	850	1.60	2220
0100F3	Moderate insulation	0.42	0.45	0.90	1033	1.00	1687

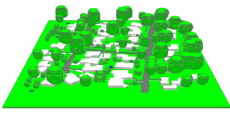
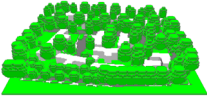
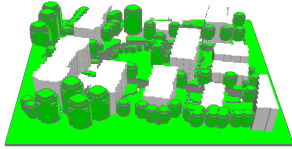


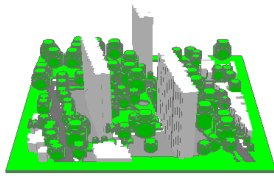
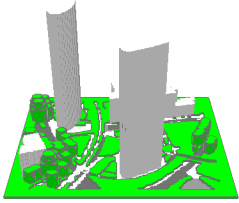
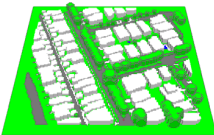
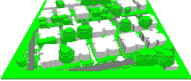
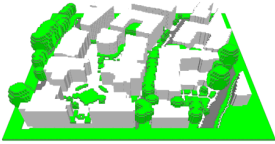
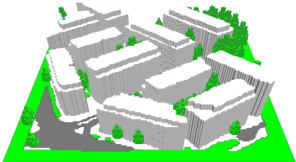
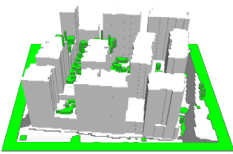
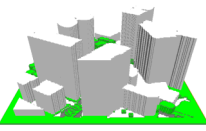
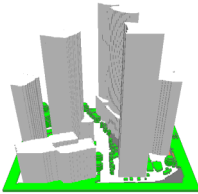
Table 5. The urban surfaces albedo and emissivity.

Code	Name	Albedo	Emissivity	Used in OT	Used in CT
0100ST	Asphalt Road	0.2	0.9		2
0100PD	Concrete Pavement Dark	0.20	0.90	1-6-7	1-3
0100PG	Concrete Pavement Gray	0.50	0.90	1-3-4-5-6-7	1-2-3-7
0100PL	Concrete Pavement Light	0.80	0.90	1-3-4-5-7	1-2-3-5-7
0100Q3	Cool Pavement	0.50	0.90	1-2-3-4-5-6-7	1-2-3-4-5-6-7
0100Q5	Cool Asphalt Road	0.55	0.90	1-2-3-4-5-6-7	1-2-3-4-5-6-7
0100KK	Brick road (red stones)	0.3	0.9		2-7
0100GG	Dark Granit Pavement	0.3	0.9		3
0100WW	Deepwater (swimming pools)	0.00	0.96	1-4	1-

Table 6. The vegetation characteristics.

Code	Name	OT	CT
0100XX	Grass 25 cm aver. Dense	1-2-3-4-5-6	1-2-3-4-5-6-7
0100H2	Hedge dense, 2 m	1-3-4-5-6	7
0100H4	Hedge dense, 4 m	1	
01ALDM	Conic, large trunk, dense, medium (15 m)		4
01ALDL	Conic, large trunk, dense, large (25 m)		4
01ALDS	Conic, large trunk, dense, small (5 m)		4
01CMSS	Cylindric, medium trunk, sparse, small (5 m)		5
01CSSS	Cylindric, small trunk, sparse, small (5 m)		5
01CLSS	Cylindric, large trunk, sparse, small (5 m)		5
01CLDM	Cylindric, large trunk, dense, medium (15 m)	1-3-4-5-6	1-2-3-5-6-7
01CLDS	Cylindric, large trunk, dense, small (5 m)	1-3-4	1-2-3-5-6-7
01CSDS	Cylindric, small trunk, dense, small (5 m)	3-4-6	1
01CLDL	Cylindric, large trunk, dense, large (25 m)	3-4	1-2-3-7
01CSDM	Cylindric, small trunk, dense, medium (15 m)	3-4-6	1
01CMDM	Cylindric, medium trunk, dense, medium (15 m)	1-4-5-6	
01CLDL	Cylindric, large trunk, dense, large (25 m)	1-2-6	7
01HLDL	Heart-shaped, large trunk, dense, large (25 m)	1	2
01PSDS	Palm, small trunk, dense, small (5 m)		7
01CMDS	Cylindric, medium trunk, dense, small (5 m)	1-4-5	7
01PSDS	Palm, small trunk, dense, small (5 m)	1	
01PLDS	Palm, large trunk, dense, small (5 m)	2-4-6	3-7
01PLDM	Palm, large trunk, dense, medium (15 m)	1-4	6-7
01PLDL	Palm, large trunk, dense, large (25 m)	2	6
01OMDS	Cylindric, medium trunk, dense, small (5 m)		6
01OLDM	Cylindric, large trunk, dense, medium (15 m)	2-4	6
01CMDL	Cylindric, medium trunk, dense, large (25 m)	1-3-4-6	
01OLDS	Cylindric, large trunk, dense, small (5 m)	2	6
01OLDL	Cylindric, large trunk, dense, large (25 m)	2	6
01SLDS	Spherical, large trunk, dense, small (5 m)	6	
01SMSL	Spherical, medium trunk, sparse, large (25 m)	6	
01SMDS	Spherical, medium trunk, dense, small (5 m)	6	
01CLSM	Cylindric, large trunk, sparse, medium (15 m)	6	
01SMDM	Spherical, medium trunk, dense, medium (15 m)	6	

Table 7. The models developed in ENVI-met for all typologies and the mitigated scenarios.

Open Precincts				
Type	OT1: Open Single Dwellings	OT2: Open Low Rise	OT3: Open Low/Medium Rise	
Envimet Model				
	OT4: Open Medium rise	OT5: Open Medium/high rise	OT6: Open High rise 1	OT7: Open High rise 2
ENVI-met Model				
Compact precincts				
Type	CT1: Compact single dwellings	CT2: Compact Low rise	CT3: Compact Low/Medium Rise	CT4: Compact Medium rise
ENVI-met Model				
	CT5: Compact Medium/high rise	CT6: Compact High rise 1	CT7: Compact High rise 2	
ENVI-met Model				

5. Simulation Results

Simulations are performed for both the unmitigated and mitigated cases. The basic values of the urban configuration and mitigated scenarios are tabulated in Table 8. The simulation results are included in the following subsections.

Table 8. Basic Values of the urban configuration used for the base run and mitigation simulations.

Urban Canopy Parameters			Base Run and Unmitigated Scenario		Mitigated Scenario Values		
Urban Categories	Cat	Building Height	Urban Fraction	Roof Albedo	Road Albedo	Roof Albedo	Roof Albedo
Commercial Business Dist.	CBT	28	0.95	0.15	0.08	0.6	0.6
High Density	HD	13	0.66	0.15	0.08	0.6	0.6
Medium Density	MD	6	0.62	0.15	0.08	0.6	0.6
Low Density	LD	4	0.55	0.15	0.08	0.6	0.6
Industrial	IN	6	0.60	0.6	0.08	0.6	0.6

5.1. Simulation Results for the Unmitigated Cases

Simulations have been performed using an unmitigated weather file for the year 2050. Furthermore, the various ENVI-met model's settings are set to the base case with no mitigation techniques. The urban canopy settings for all unmitigated simulations are: Road Albedo = 0.08, Roof Albedo = 0.15, a limited number of trees, and no water sprinklers in the precincts for each precinct, the air temperature, surface temperature, wind speed, and thermal comfort indices are extracted.

For all precincts, the ambient temperature ranges are tabulated in Table 9. For all CT cases, the thermal comfort is mostly improved in the shaded areas while there is moderate to strong heat stress. The wind speed is significantly reduced between the buildings.

Table 9. The results of the unmitigated cases for 14:00.

Precinct	Air Temperature Range (°C)	Maximum Wind Speed (m/s)	Surface Temperature Range (°C)	UTCI Range (°C)
CT1	31.9–35.3	2	26.6–57.8	35.0–43.6
CT2	31.8–34.9	2.8	25.8–55.9	34.6–43.2
CT3	31.7–35.3	2.3	27.4–57.0	34.5–43.7
CT4	32.2–35.6	3.2	27.7–57.0	34.5–43.8
CT5	32.0–35.0	4	26.1–56.3	33.8–43.4
CT6	31.0–34.6	3.4	24.4–55.6	31.9–41.5
CT7	31.5–34.4	5.1	24.5–55.4	30.9–41.5
OT1	32.1–34.7	1.8	25.5–56.2	35.2–43.4
OT2	31.9–35.2	2.1	26.1–57.0	34.4–43.5
OT3	31.9–35.2	2.4	26.0–58.4	34.1–44.0
OT4	32.2–34.6	2.3	24.3–56.6	34.9–43.5
OT5	31.6–34.8	3.7	25.9–57.1	34.0–43.0
OT6	32.3–34.7	3.4	25.4–56.6	32.9–42.9
OT7	31.9–34.9	4.1	25.5–56.8	32.9–42.6

Indicatively the air temperature distribution for CT1 and OT7 are depicted in Figures 1 and 2 respectively. The air movement around buildings for CT5 is illustrated in Figure 3 and the surface temperature in Figure 4.

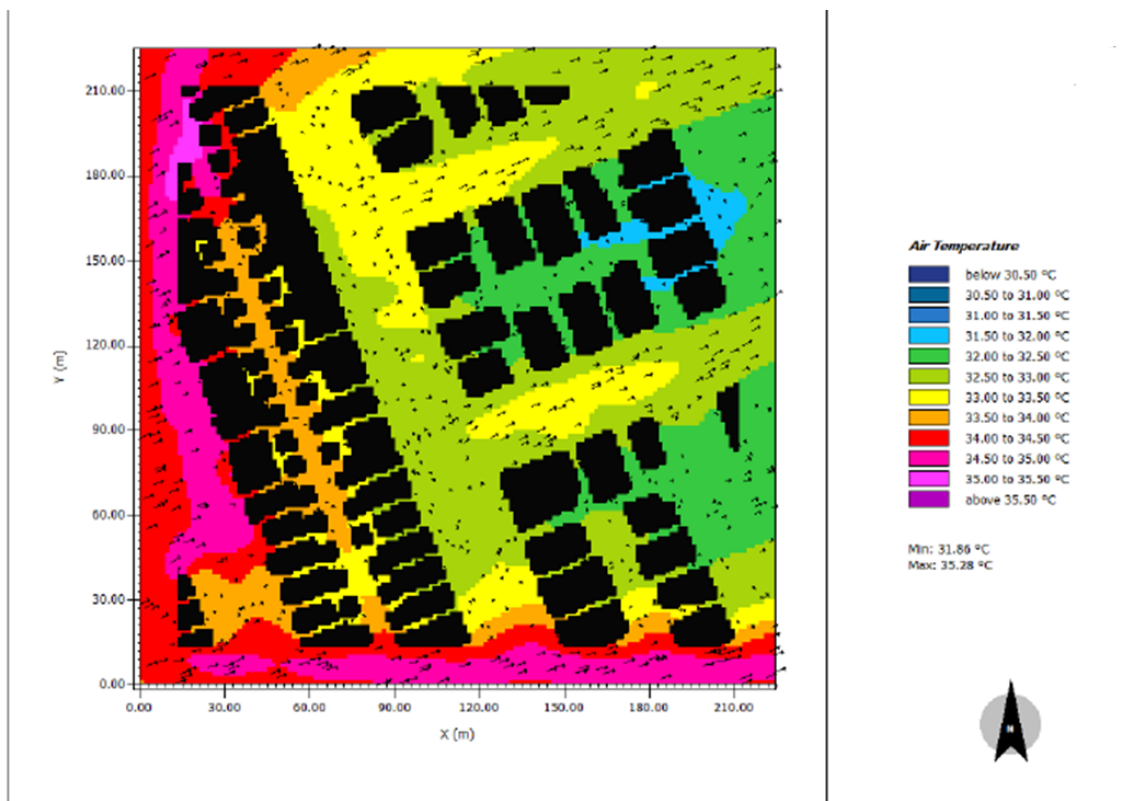


Figure 1. The air temperature distribution under unmitigated conditions for CT1 at 14:00.

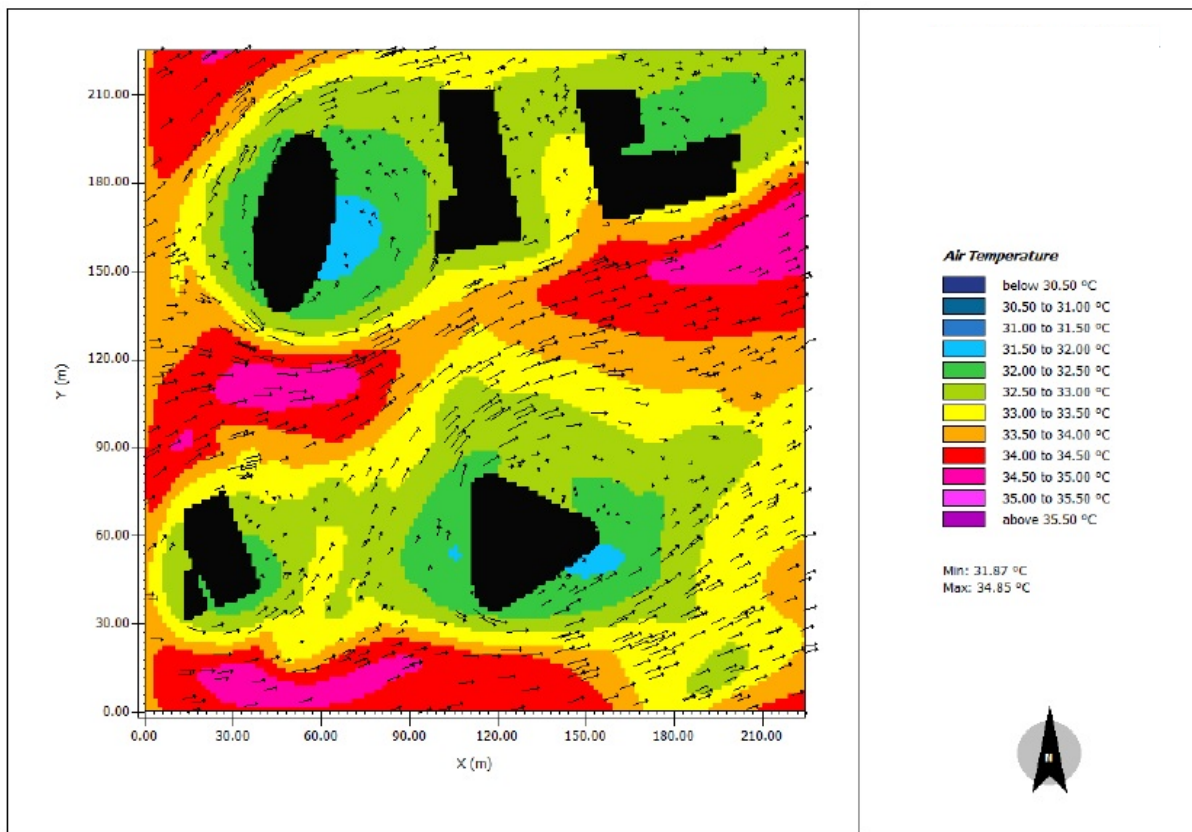


Figure 2. The air temperature distribution under unmitigated conditions for OT7 at 14:00.

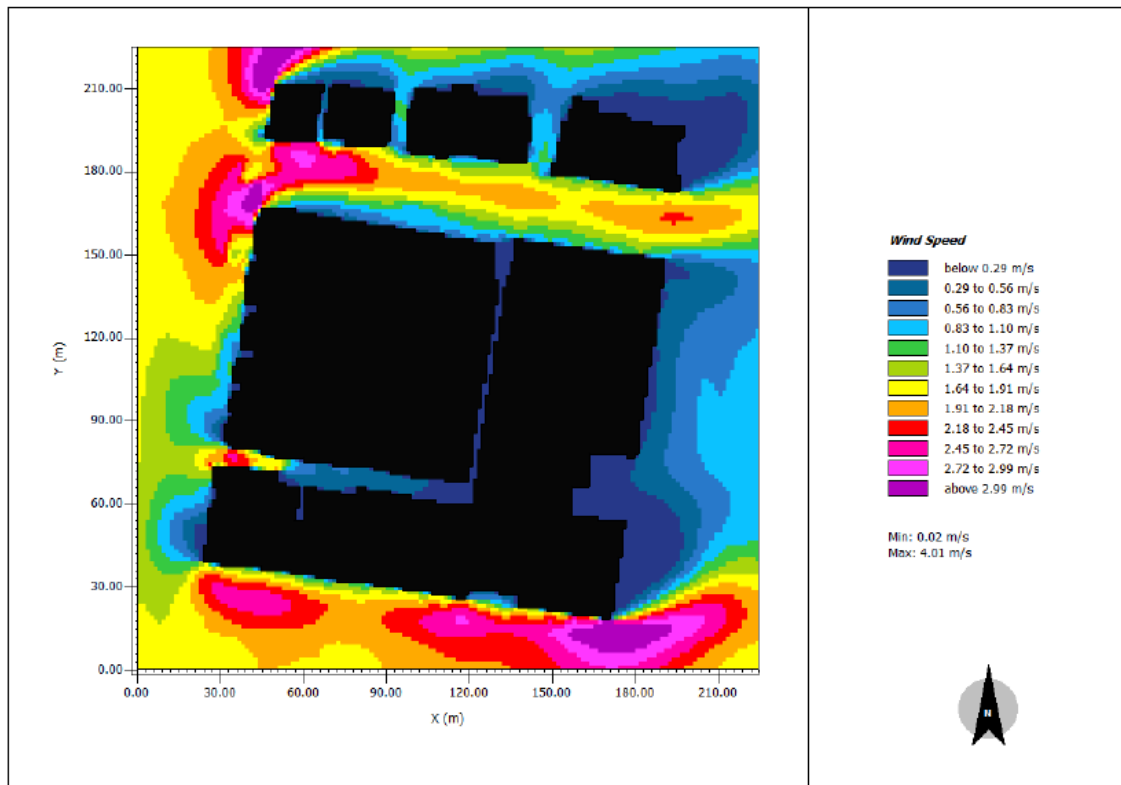


Figure 3. The wind speed distribution under unmitigated conditions for CT5 at 14:00.

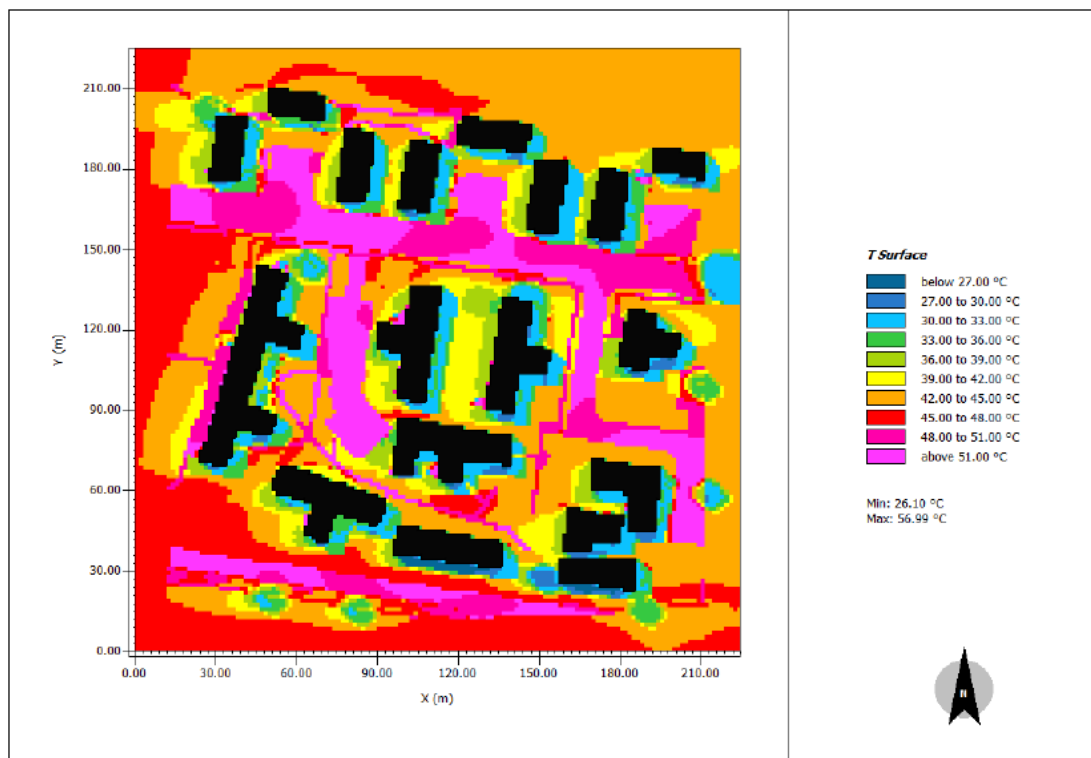


Figure 4. The surface temperature under unmitigated conditions for OT2 at 14:00.

5.2. Simulation Results for the Mitigated Cases

The mitigated scenario is based on the 2050 land use and climate. It assumes the implementation of mitigation technologies in the whole Sydney area. The RCP4.5 Future Scenario [39,40] dataset has been used for the Urban Plan simulation. It includes (a) increased building density based on future projections (b) new Urban Growth Areas (c) increased Anthropogenic Heat Flux (d) 2 million irrigated trees planted in the “Third City” area and 3 million irrigated trees planted in the rest of Sydney (e) increased albedo (0.6) of urban impervious surfaces and (f) Water in the landscape. The mitigated scenario values are tabulated in Table 8.

Table 10 shows the statistical summary of the ambient temperature at 14:00. CT1 has the maximum ambient temperature followed by CT4 and CT5. The minimum ambient temperature is 27.5 °C in CT6. The lowest 25th percentile of temperature data is 29.7 °C, observed in CT6 and OT6. The 95th percentile of data is 33.0 °C in CT4. The average ambient temperature in CT layouts is higher than that in OT layouts.

Table 10. Statistical summary of the ambient temperature results at 14:00 for all precincts.

Layout	Ambient Temperature Statistical Results (°C)						Percentiles					
	TMax ¹	TMin ¹	Mean	Median	Std.	TMax ²	TMin ²	25	50	75	90	95
OT1	33	27.9	31	30.6	0.9	33	26.3	30.3	30.6	31.8	32.4	32.5
OT2	32.2	28.5	30.4	30.3	0.8	32.5	25.1	29.9	30.3	30.8	31.4	31.8
OT3	32.7	27.7	30.8	30.8	1	32.7	24.8	30	30.8	31.5	32.1	32.4
OT4	32.7	29.8	31.3	31.3	0.9	32.9	22.1	30.9	31.3	31.6	32.4	32.6
OT5	32.9	28.8	31.1	31	0.8	32.9	26.6	30.5	31	31.7	32.3	32.6
OT6	32.7	27.7	30.2	30.5	1.7	32.7	18.6	29.7	30.5	31.1	31.8	32
OT7	33	29.2	31.2	31.1	0.8	33.1	26.3	30.7	31.1	31.6	32.2	32.5
CT1	33.4	28.4	31.1	30.8	1	33.4	25.8	30.4	30.8	31.8	32.7	32.8
CT2	33	28	31.2	31.2	1	33	25.7	30.5	31.2	32.1	32.5	32.6
CT3	32.9	27.9	31	30.7	0.9	32.9	27.1	30.2	30.7	31.8	32.4	32.7
CT4	33.2	29.3	31.4	31.3	0.8	33.2	26.3	30.9	31.3	32	32.5	32.7
CT5	33.2	28.3	31.5	31.3	1	33.2	27.2	30.7	31.3	32.3	32.8	33
CT6	32.7	27.5	30.4	30.2	1	32.7	24.5	29.7	30.2	31.1	31.8	32
CT7	32.4	28.2	30.4	30.2	0.8	32.4	27.1	29.8	30.2	31	31.6	31.9

¹: The minimum and maximum excluding outliers. ²: The absolute minimum and maximum temperature data.

The ambient temperature difference of the mitigated versus the unmitigated simulations in each precinct is reported in Table 11. The average reduction of ambient temperature ranges between 2.1 °C ± 0.4 and 3.3 °C ± 1.5°C. The minimum reduction of ambient temperature is observed in CT7 and the maximum in OT6.

Table 11. Ambient air temperature differences of the unmitigated versus the mitigated scenarios for all precincts.

	CT1	CT2	CT3	CT4	CT5	CT6	CT7	OT1	OT2	OT3	OT4	OT5	OT6	OT7
Mean	2.20	2.22	2.32	2.14	2.13	2.13	2.09	2.33	3.04	2.78	2.39	2.27	3.26	2.16
Std.	0.48	0.69	0.63	0.70	0.61	0.52	0.37	0.51	0.68	0.73	0.90	0.89	1.49	0.56
Minimum	1.42	1.41	1.64	1.10	1.57	1.37	1.54	1.48	1.88	1.62	1.21	0.93	1.69	0.81
Maximum	8.18	8.17	7.59	6.84	7.25	7.74	5.20	7.33	8.76	9.59	11.98	7.70	14.50	7.35

The charts of the ambient temperature differences are depicted in Figure 5. The maximum air temperature differences occur close to the water sprays and these high-temperature differences extend beyond the point of water spray position depending on the wind direction and the typology examined.

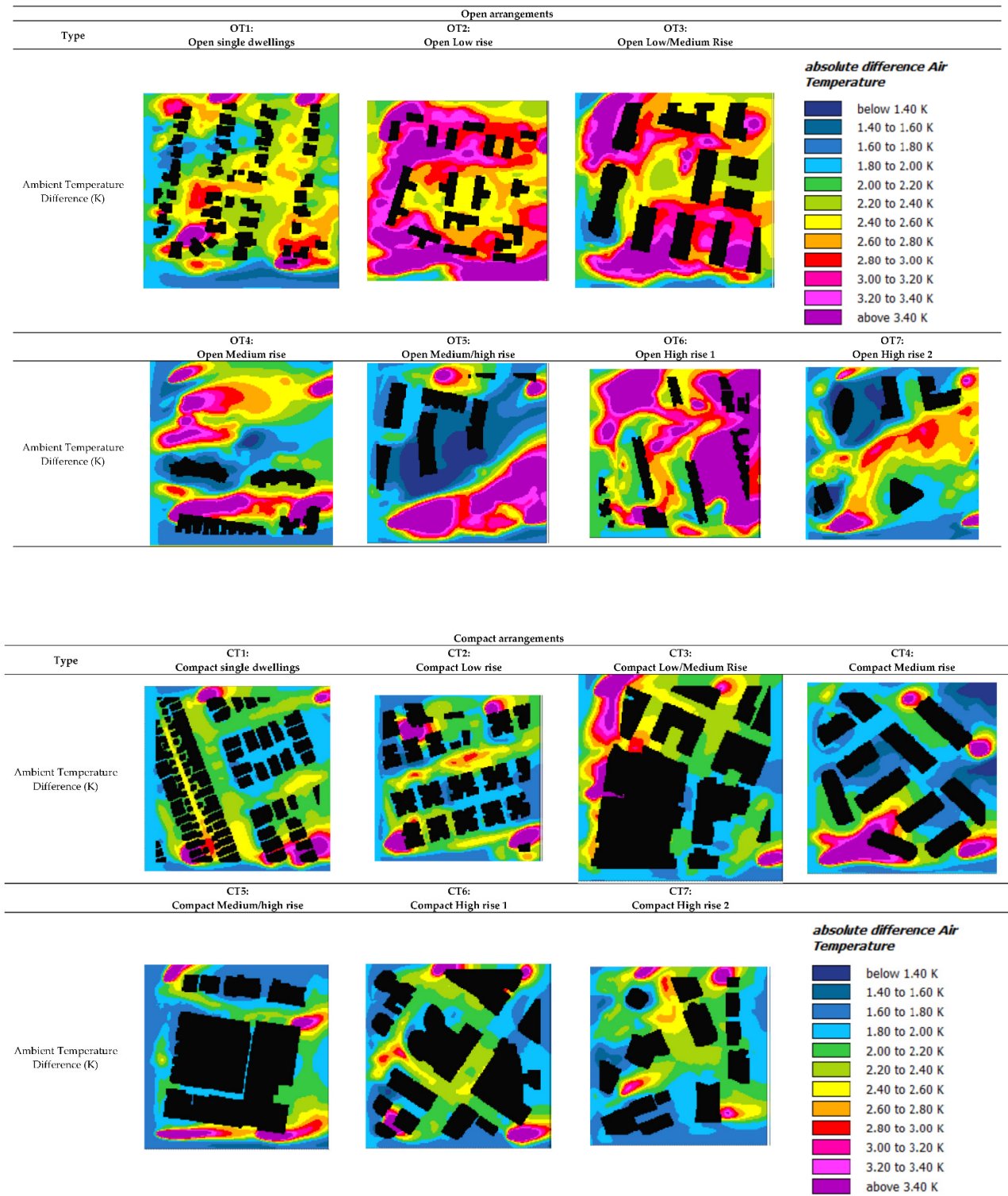


Figure 5. Ambient Temperature Comparison Charts for mitigated vs unmitigated cases and 14:00.

The charts of the surface temperature differences are depicted in Figure 6. The areas shaded by buildings and trees present lower surface temperatures.

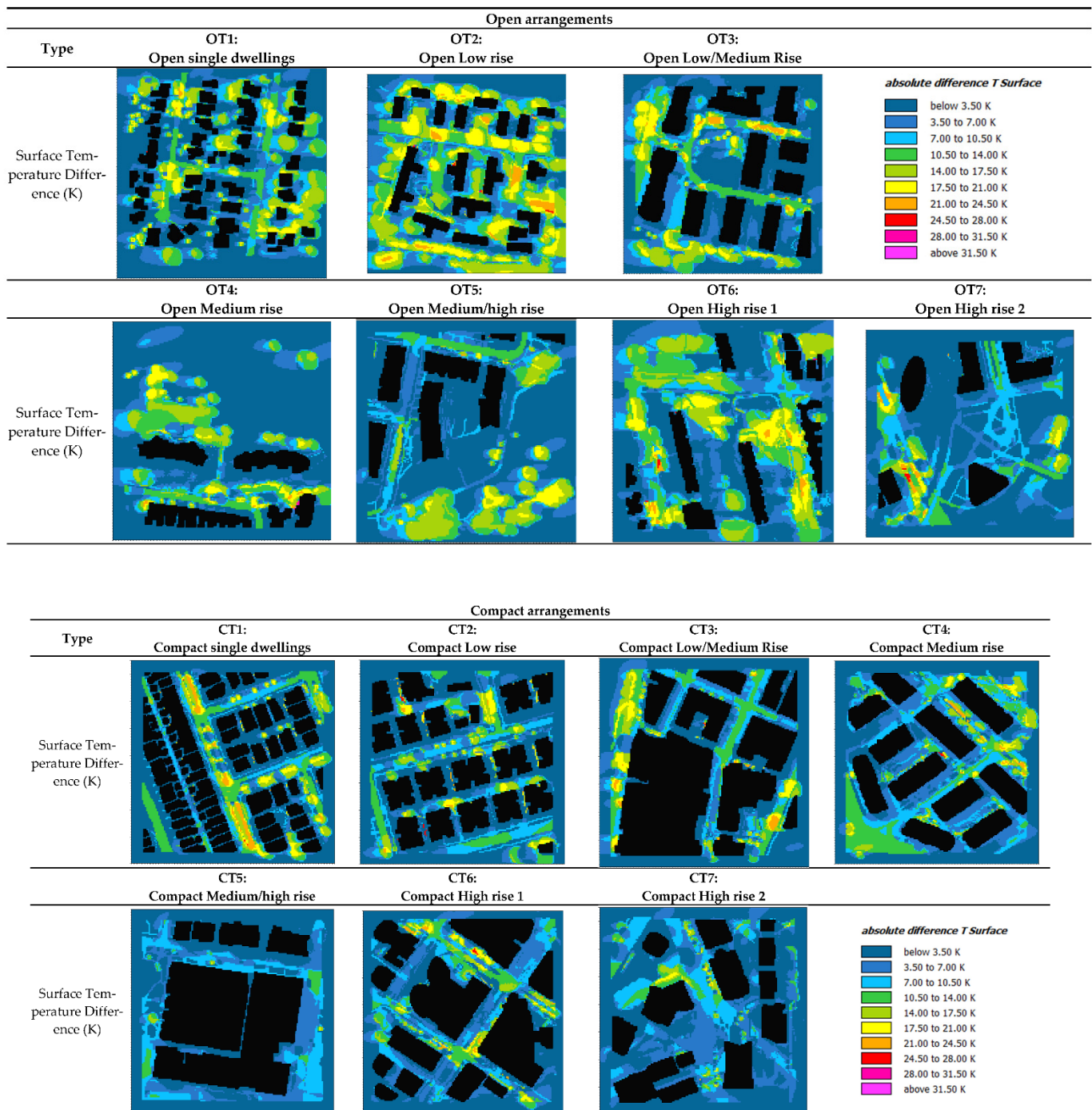


Figure 6. Surface Temperature Comparison Charts for mitigated vs unmitigated cases and 14:00.

The ambient temperature, surface temperature, and thermal comfort results for the mitigated versus the unmitigated scenarios are similar to those extracted from other research published and used the ENVI-met model [41–44].

6. Analysis of Results and Discussion

Based on the simulation results a more detailed analysis is performed. The cooling potential of each of the 14 studied precincts is evaluated using the 'Gradient of the

Temperature Decrease along the Precinct Axis' (GTD) parameter. The GTD parameter measures the average temperature decrease along the axis of the canyon that is closer to the wind direction.

In the present study, the angle of the wind speed direction (250°) with the X-axis is smaller than the angle with the Y-axis, thus the GTD parameter is calculated along the X-axis.

The climatic parameters in each precinct are calculated for a 224×224 cells grid. For each parameter, W , its average value is defined as $W(X_i, Y_{1-224})$, corresponding to one X cell and all the 224 Y cells of the same X value. For example, for the cell $X = 3$, the sum of the W values corresponding to cells with $X = 3$ and $Y = 1$ to 224, is calculated and divided by 224. In case cells do not include numerical values of the parameter W (if the area is covered by buildings), then the corresponding cells are not considered.

The GTD for the average distribution of ambient temperature, and wind speed, is calculated along the axis X. The $GTD(x)$, is calculated as the average difference between the initial and the final value of the ambient temperature along the X-axis:

$$GTD(x) = \frac{T_{(average\ x=1)} - T_{(average\ x=224)}}{224} \quad (1)$$

$GTD(x)$ counts for the temperature decrease along the X-axis per meter of length of the precinct and expresses the potential of the precinct to mitigate the ambient overheating along the axis closer to the wind direction. The procedure is followed for all precincts with mitigation and without mitigation.

Indicative results are shown for CT1 and OT3 in Figures 7 and 8 respectively while all results are tabulated in Table 12. For the mitigated scenarios the GTD varies between 0.01 K/m to 0.004 K/m. In the unmitigated scenarios, the GTD varies between 0.0093 K/m to 0.0024 K/m. The maximum expected temperature difference between precincts of about $40,000 \text{ m}^2$ with different layouts, building typologies, and open spaces types, where the same mitigation measures are implemented, may be close to 0.9 K, for a reference ambient temperature of 32°C and a wind speed of about 2 m/s. Moreover, the maximum expected temperature difference between precincts of about $40,000 \text{ m}^2$, without mitigation, is close to 1.5 K, for reference ambient temperature of 33°C , and wind speed of about 2 m/s.

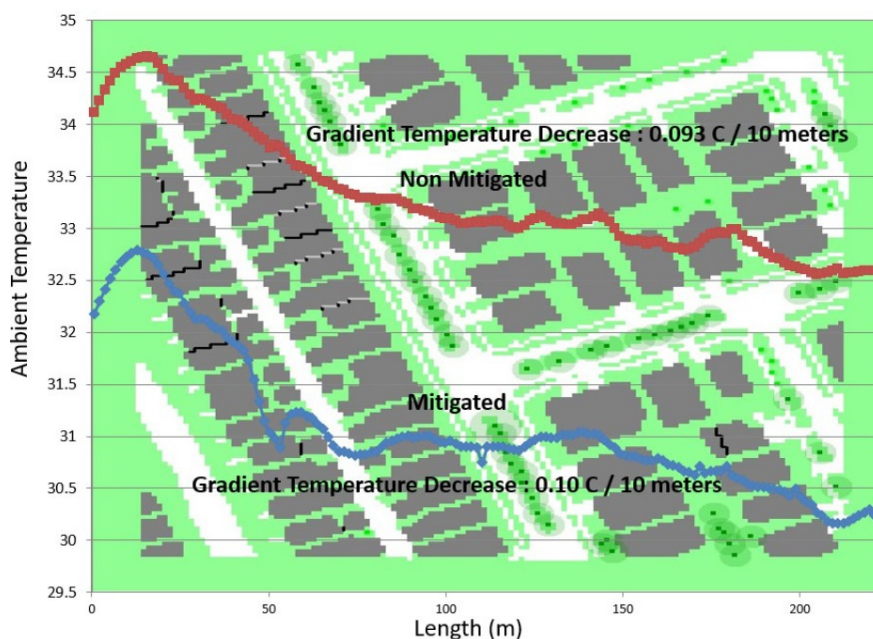


Figure 7. The GTD for the CT1 precinct for both mitigated and unmitigated scenarios is shown in the ENVI-met configuration.

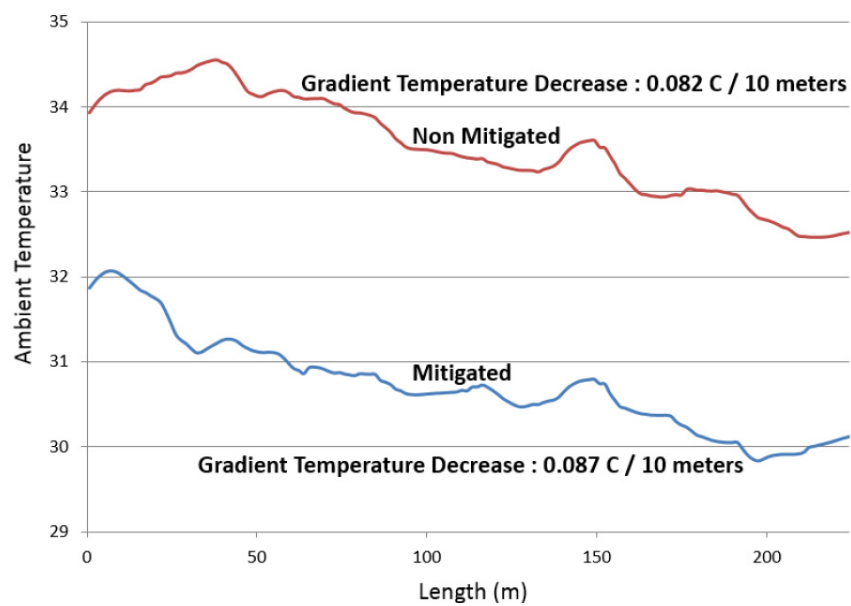


Figure 8. The GTD for OT3 precinct for both mitigated and unmitigated scenarios.

Table 12. The Gradient Temperature Decrease at the wind flow direction for all precincts.

Mitigated GTD across the Precincts (K/100 m)						
1.1	0.95	0.90	0.87	0.84	0.84	0.83
CT1	OT6	OT1	OT3	CT6	OT2	CT2
0.80	0.77	0.70	0.68	0.58	0.42	0.4
OT4	CT3	OT5	CT4	CT5	CT7	OT7
Unmitigated GTD across the Precincts (K/100 m)						
0.93	0.82	0.79	0.75	0.73	0.73	0.70
CT1	OT3	CT2	CT6	CT3	OT1	OT6
0.69	0.66	0.60	0.53	0.50	0.30	0.24
OT2	CT4	OT4	OT5	CT5	CT7	OT7

The wind flow regimes of each precinct are depicted in Figure 9. For each precinct, the areas are divided into different zones that are either parallel or perpendicular to the wind speed. In Figure 9 the GTD is also included.

For CT1 the ambient temperature is strongly related to the wind speed. As the advection heat increases with higher wind speeds, the ambient temperature increases too. The sections of zone 1, in both CT2 and CT3, provide low advection and good solar protection thus highly contributing to increasing the cooling gradient. Zones 2 and 3 of CT2 are parallel to the wind direction; they present however a significant cooling rate that is attributed to the intensive planting mitigation. The CT3 zone 2 and CT4 zone 2 sections, despite being perpendicular to the wind direction, present a low average wind speed and a substantial cooling rate because of the intensive planting considered. In CT4 the sections of zone 1, specifically canyon 1a and 1c, provide high advection air flows, contributing highly to ambient temperature increase. CT5 precinct is densely built with high-rise buildings. In Zone 1 of CT5, the high advection air flows contribute highly to increasing the ambient temperature, while the impact of zone 2 is negligible. Similarly, in canyon 2a in zone 2 of CT6 as well as in CT7 high advection flows are observed that result in increased ambient temperature. In all precincts, except CT5, the combination of mitigation measures, namely cool pavements, cool roofs, and vegetation, results in a substantially ambient temperature

decrease. Especially significant is the mitigation impact of tree shading. In CT5, due to its density, fewer trees are used, and the high-rise buildings minimize the cool roof impact.

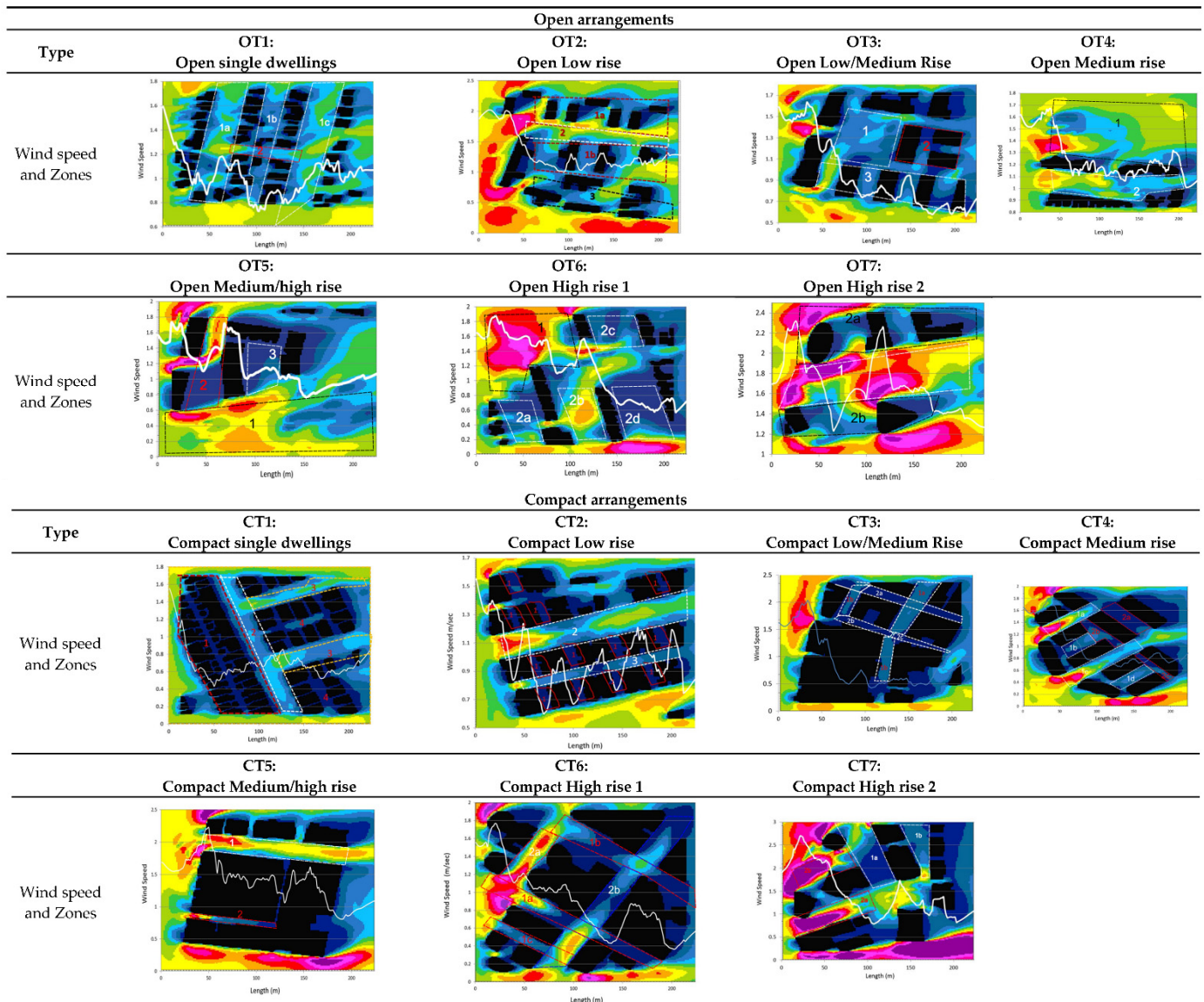


Figure 9. Wind speed in all precincts.

In the OT1 precinct, the zone 1 sections provide high advection air flows and contribute highly to increasing the temperature in the precinct. In OT2 the building arrangement provides wind shading resulting in lower wind speeds and lower heat advection. Similar conditions are observed in OT3 zones 2 and 3. In both OT2 and OT3, solar shading is not optimized resulting in high surface temperatures in the non-shaded zones. The combination of cool pavements, cool roofs, and vegetation results in a substantial decrease in the ambient temperature. Especially significant is the mitigation impact of tree shading. No wind or solar shading is present in the OT4 and OT7 configurations. In these two precincts, the mitigation measures contribute to the ambient temperature decrease along the canyon axis. Zone 3 in OT5 configuration, is well protected from the wind. As a result, the wind speed and ambient temperature are reduced. Solar shading, however, is not optimized, and the temperature decrease along the canyon axis is owed to the mitigation measures. The OT6 configuration partly benefits from wind shading, while trees offer insignificant

solar shading. In this case, too, the mitigation measures result in a temperature decrease along the precinct axis.

Analysis of the results shows that advection heat transfer is prominent in the precincts. The heat flux is strongly related to the wind and the GTD values.

The advected heat is a function of the open spaces across the precinct where wind can flow and of the corresponding wind speed.

Given that the analyzed precincts are of square form, an average cross-section, $S_{average}$, is calculated as:

$$S_{average} = [(1 - BAR) \cdot A]^{0.5} \quad (2)$$

where: BAR is the Built Area Ratio of each precinct and A is the total area of the precinct.

The average wind speed is calculated for the whole area of the precinct, $V_{average}$.

The average advected heat, ($Q_{average}$), for each precinct can be approximated with the following equation:

$$Q_{average} = S_{average} \cdot V_{average} \quad (3)$$

The GTD value of each precinct is observed to have a strong correlation with the corresponding $Q_{average}$ for both the mitigated and non-mitigated precincts (Figure 10).

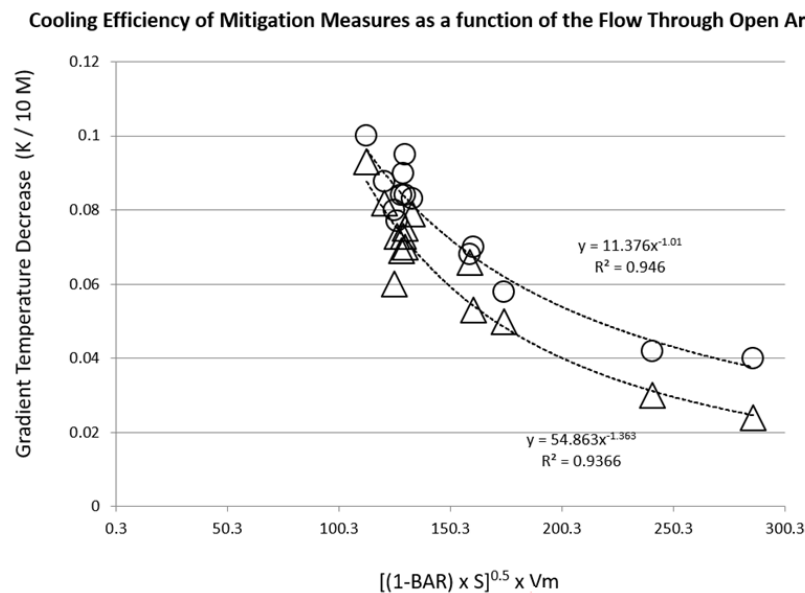


Figure 10. Cooling Efficiency of Mitigation Measures as a function of the Flow-Through Open Areas.

The correlation has the form:

$$GTD(i) = a \cdot Q_{average}^b, \quad (4)$$

The a , b values are extracted from Figure 10. The corresponding R^2 values for both the mitigation and non-mitigation scenarios are close to 0.9 (see Figure 10).

The correlation clearly shows that when the heat advection in the precinct is lower, the GTD is higher, meaning that the protection against overheating is higher.

A strong correlation is also found between the ratio of the average wind speed in the precinct $V_{average}$, and the incident wind speed in the limits of the precinct, V_{inc} with the average aspect ratio of the precinct, H/W .

Where: H is the average height of the buildings and W is the *average* width of the streets

The correlation is expressed with the equation:

$$\frac{V_{average}}{V_{inc}} = a_1 + b_1 \cdot H/W \quad (5)$$

The parameters a_1 and b_1 can be taken from Figure 11.

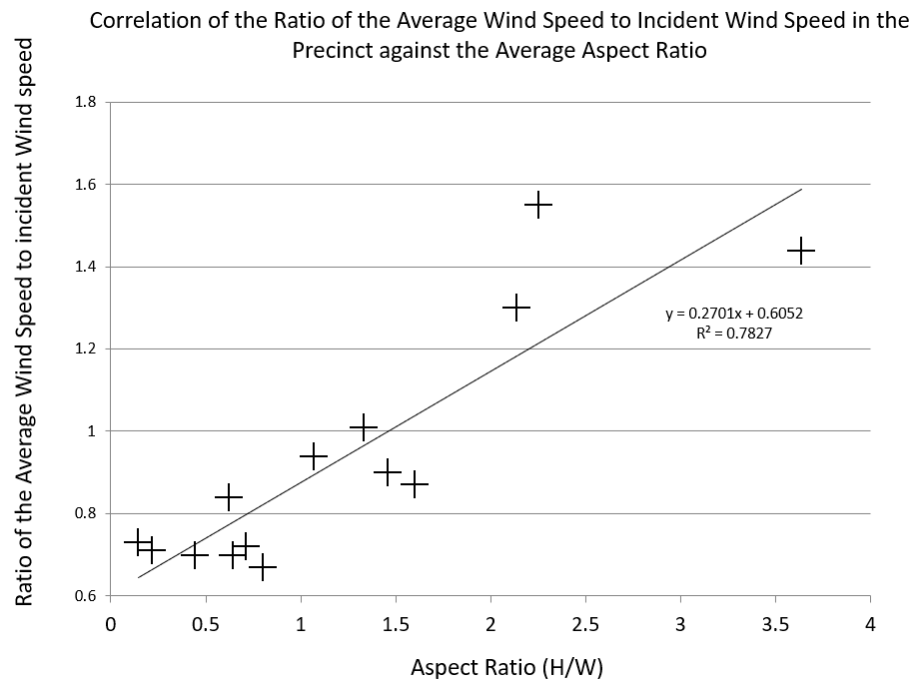


Figure 11. Correlation of the Ratio of the Average Wind Speed to Incident Wind Speed in the Precinct against the Average Aspect Ratio.

A comparison of the GTD values for the mitigated and non-mitigated scenarios, shows clearly that the mitigation measures, (vegetation, evaporation, and cool materials), increase significantly the GTD of the precincts as well as their cooling capacity.

In the mitigated scenarios, the total $GTD_{(total, mit)}$ can be attributed to (a) The mitigation measures and (b) The layout of the precinct. In this case, it can be written that:

$$GTD_{total, mit} = GTD_{mitigation} + GTD_{layout} \quad (6)$$

For a given advection rate $Q_{average}$, the GTD_{layout} can be calculated from the corresponding expression of Equation (4), and the specific contribution of the mitigation can be calculated from Equation (6).

Based on the analysis of the role of $Q_{average}$, it can be concluded that the cooling potential of the precincts based on their layout is increased when advection is low and decreases as advection is rising.

Moreover, a quite strong correlation is observed between the $GTD_{mitigation}$ and the Built Area Ratio, (Figure 12). As the Built Area Ratio increases, the contribution of the mitigation measures to the cooling rate of the precincts decreases, since less space is available for implementing the mitigation measures.

Cooling Efficiency of Mitigation Measures as a function of the Built Area Ratio

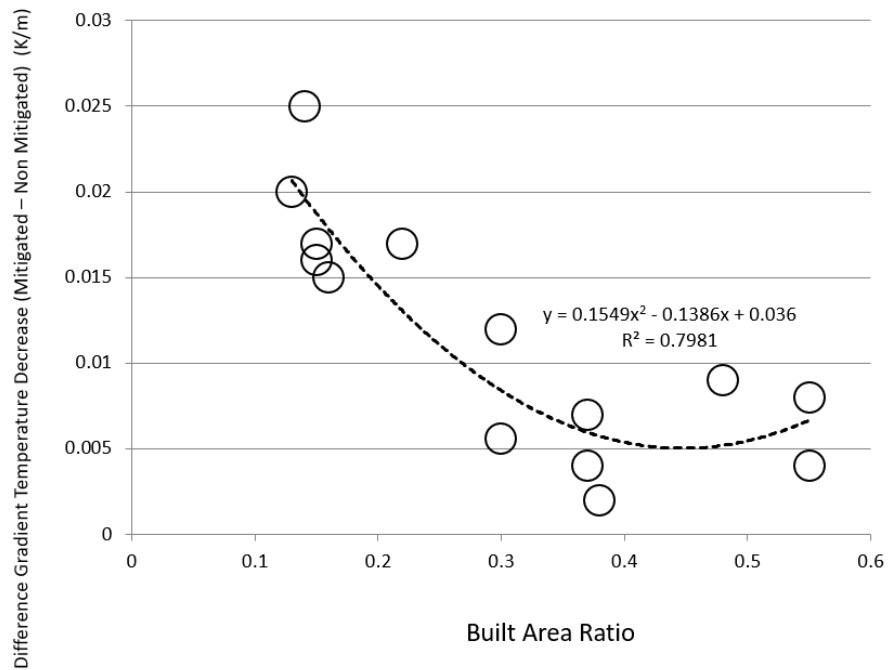


Figure 12. Cooling Efficiency of Mitigation Measures as a function of the Built Area Ratio.

A clear and strong correlation is found between the GTD of all the precincts with and without mitigation, and their corresponding average aspect ratio, (H/W), (Figure 13). The relation is:

$$GTD(i) = a_2 + b_2 HW \tag{7}$$

where a_2 and b_2 are coefficients provided in Figure 13.

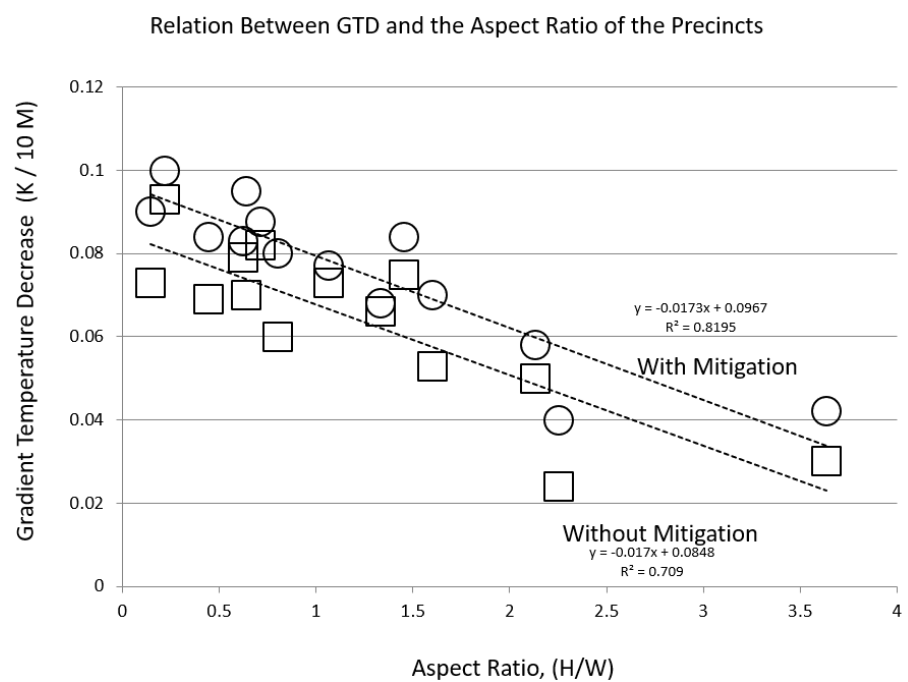


Figure 13. Relation between GTD and the Aspect Ratio of the Precincts.

As shown in Figure 13, the higher the aspect ratio of a precinct the lower the cooling potential and *GTD*. This is expected, as (a) the application of cool roofs in high-rise buildings has a lower mitigation impact and (b) in canyons of high aspect ratios the wind speed is high and results in a much higher advection rate.

Both prediction methods proposed to calculate the *GTD* of the mitigated and non-mitigated precincts are of sufficient accuracy. Figures 14 and 15 compare the predicted *GTD* values, calculated with the two methods, against the original data for the mitigated and the non-mitigated precincts. The average relative prediction error of both methods for the mitigated precincts is close to 10%. For the non-mitigated precincts, the average prediction error of the method based on the aspect ratio is close to 17%, while the corresponding error of the method based on the estimation of the advection rate is close to 12%.

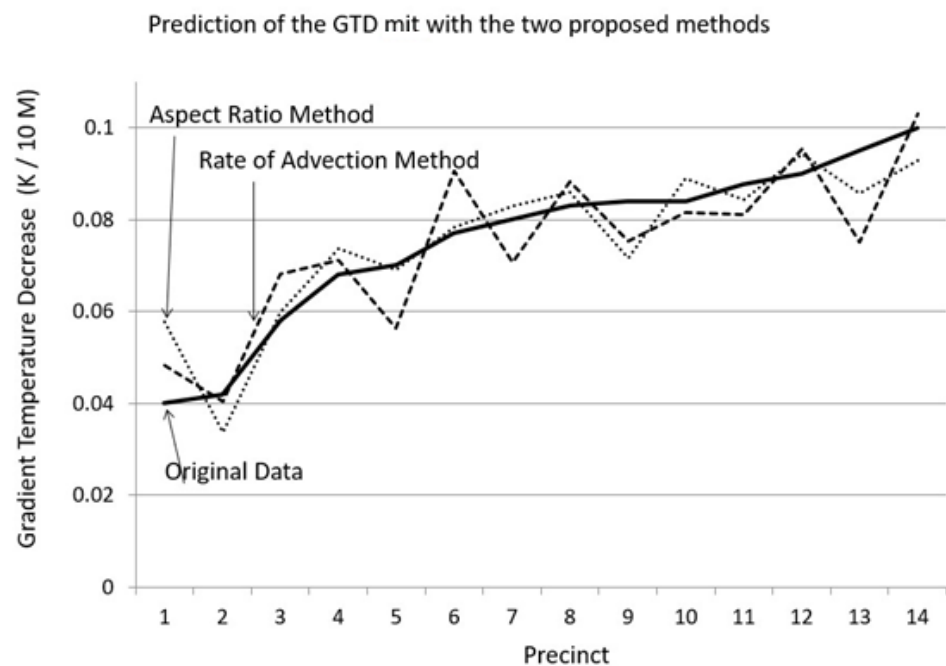


Figure 14. Prediction of the $GTD_{mitigation}$ for the mitigated scenarios with the two proposed methods.

The advection rate in the precincts is highly dependent on the canyon orientation and aspect ratio. The wind speed in canyons with an axis vertical or oblique to the wind direction presents a lower wind speed is lower compared to wind speed in canyons with a parallel axis to the wind direction. This depends highly on the aspect ratio, (H/W), of the canyons, as derived by Oke [45]. For canyons vertical or oblique to the wind direction, a high H/W value > 0.8 signifies that the flow is under a skimming regime and corresponds to a local vortex inside the canyon, and a bypass of the flowing air above the height of the buildings. For H/W values between 0.8 and 0.3, the flow is the wake interface, and for lower values is isolated roughness [45].

For all canyons of the precincts that have their axis vertical or slightly oblique to the wind direction, a strong correlation between the average wind speed in the canyon, $V_{average}$, and the aspect ratio (H/W , is found (Figure 16). The relation has the form:

$$V_{average} = 0.2046 \cdot \left(\frac{H}{W} \right)^{-1.745} \quad (8)$$

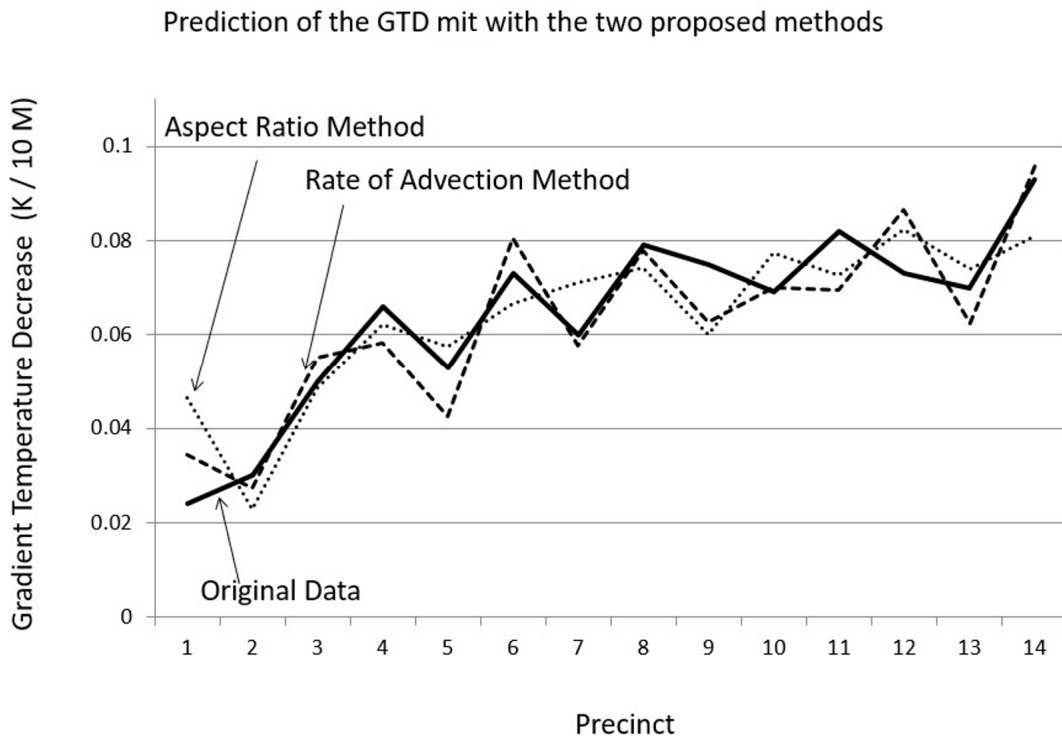


Figure 15. Prediction of the $GTD_{mitigation}$ for the unmitigated with the two proposed methods.

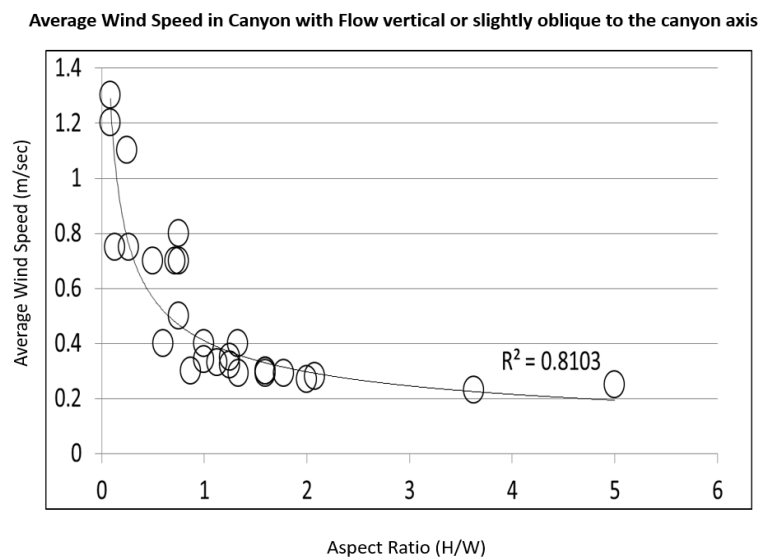


Figure 16. Average Wind Speed in Canyon with Flow vertical or slightly oblique to the canyon axis.

For all canyons that have their axis parallel to the wind direction, a strong correlation is observed between the length of the canyon and the product of the entry wind speed and width of the canyon as well as with the product of the exit wind speed with the width of the canyon (Figure 17).

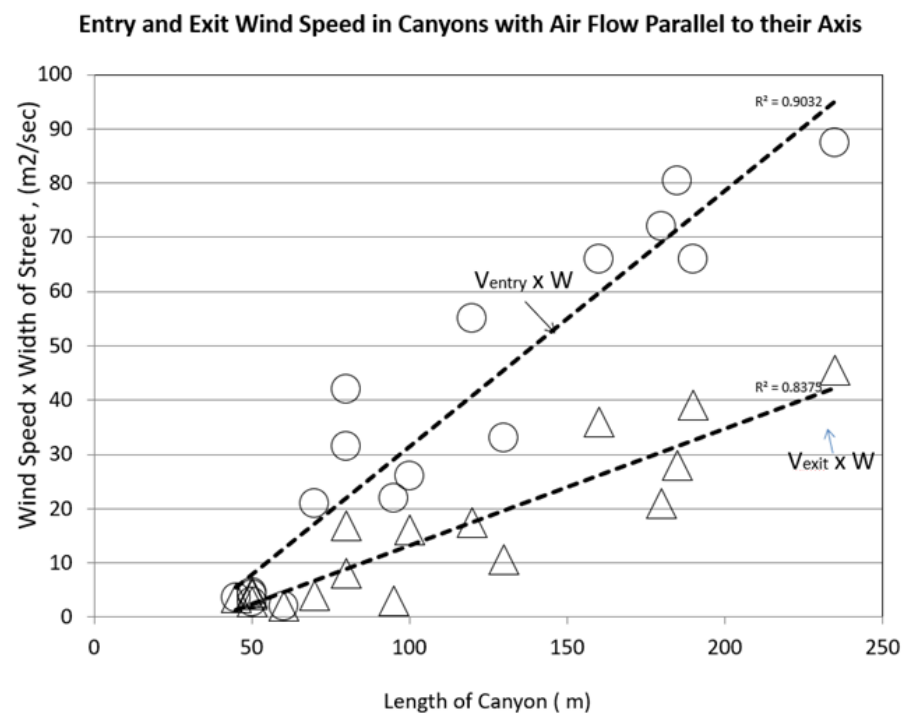


Figure 17. Entry and Exit Wind Speed in Canyons with Air Flow Parallel to their Axis.

7. Conclusions

Urban overheating causes energy, environmental, and health problems while also impacting the overall economic and cultural life of cities. The implementation of a series of mitigation measures can compensate for the negative impact of the high urban temperatures.

The mitigation measures considered in this study include the increase of greenery in the various areas, the introduction of water sprays, and the change of urban materials' albedo. The change of ambient temperature and surface temperature of the mitigated versus the unmitigated areas is significantly higher close to water sprays. The cooling potential is then studied using the GTD values along the precinct and is strongly influenced by the wind speed and direction as well as the urban form

The effect of building height, street width, aspect ratio, built area ratio, orientation, and dimensions of open spaces on the distribution of the ambient and surface temperature is further analyzed. The cooling potential of different district arrangements and building typologies is analyzed using the parameter 'Gradient of the Temperature Decrease along the Precinct Axis', GTD. The GTD measures the average temperature decrease along the X or the Y-axis of the canyon. In the mitigated precincts the GTD ranges between 0.01 K/m to 0.004 K/m. In precincts without mitigation, GTD ranges between 0.0093 K/m to 0.0024 K/m. Considering the layout of the precincts only, the cooling potential decreases when mitigation measures are implemented, compared to the cooling potential of the same precinct without mitigation.

Moreover, the main heat transfer mechanism in the precincts is advection and there is a strong relationship between the wind-caused heat flux and the GTD values. There is also a strong correlation between the GTD of all the precincts, with and without mitigation, and their corresponding average aspect ratio, (Height of buildings to Width of streets). The higher the aspect ratio of the precinct the lower the cooling potential. Finally, it is worth mentioning that a high Built Area Ratio means that less space is available for the installation of mitigation measures. Therefore, the cooling contribution of mitigation measures is lower in precincts with a higher Built Area Ratio.

Author Contributions: Conceptualization, D.K., C.B. and M.S.; methodology, S.H.; software, K.L., K.G., S.H. and S.G.; validation, D.K., K.V. and H.R.H.M.; formal analysis, R.P.; investigation, A.M.; data curation, K.G., A.M. and S.H.; writing—original draft preparation, D.K., A.M., S.G. and S.H.; writing—review and editing, M.S.; visualization, D.K. and D.P.; supervision, D.K. and M.S.; project administration, M.S.; funding acquisition, M.S. All authors have read and agreed to the published version of the manuscript.

Funding: This project is funded by the Australian Cooperative Research Council on Low Carbon Living.

Informed Consent Statement: Informed consent was obtained from all subjects involved in the study.

Data Availability Statement: Not applicable.

Conflicts of Interest: The authors declare no conflict of interest. The funders had no role in the design of the study; in the collection, analyses, or interpretation of data; in the writing of the manuscript, or in the decision to publish the results.

References

- Parker, J. The Leeds urban heat island and its implications for energy use and thermal comfort. *Energy Build.* **2021**, *235*, 110636. [[CrossRef](#)]
- Keat, W.J.; Kendon, E.J.; Bohnenstengel, S.I. Climate change over UK cities: The urban influence on extreme temperatures in the UK climate projections. *Clim. Dyn.* **2021**, *57*, 3583–3597. [[CrossRef](#)]
- Bahi, H.; Rhinane, H.; Bensalmia, A.; Fehrenbach, U.; Scherer, D. Effects of urbanization and seasonal cycle on the surface urban heat island patterns in the coastal growing cities: A case study of Casablanca, Morocco. *Remote Sens.* **2016**, *8*, 829. [[CrossRef](#)]
- Kolokotsa, D.; Psomas, A.; Karapidakis, E. Urban heat island in southern Europe: The case study of Hania, Crete. *Sol. Energy* **2009**, *83*, 1871–1883. [[CrossRef](#)]
- Martinelli, A.; Kolokotsa, D.-D.; Fiorito, F. Urban heat island in mediterranean coastal cities: The case of Bari (Italy). *Climate* **2020**, *8*, 79. [[CrossRef](#)]
- Santamouris, M. Recent progress on urban overheating and heat island research. Integrated assessment of the energy, environmental, vulnerability and health impact. Synergies with the global climate change. *Energy Build.* **2020**, *207*, 109482. [[CrossRef](#)]
- Castaldo, V.; Coccia, V.; Cotana, F.; Pignatta, G.; Pisello, A.; Rossi, F. Thermal-energy analysis of natural “cool” stone aggregates as passive cooling and global warming mitigation technique. *Urban Clim.* **2015**, *14*, 301–314. [[CrossRef](#)]
- Guha, A.; Han, J.; Cummings, C.; McLennan, D.A.; Warren, J.M. Differential ecophysiological responses and resilience to heat wave events in four co-occurring temperate tree species. *Environ. Res. Lett.* **2018**, *13*, 065008. [[CrossRef](#)]
- Bunker, A.; Wildenhain, J.; Vandenbergh, A.; Henschke, N.; Rocklöv, J.; Hajat, S.; Sauerborn, R. Effects of air temperature on climate-sensitive mortality and morbidity outcomes in the elderly; A systematic review and meta-analysis of epidemiological evidence. *EBioMedicine* **2016**, *6*, 258–268. [[CrossRef](#)]
- Santamouris, M.; Haddad, S.; Saliari, M.; Vasilakopoulou, K.; Synnefa, A.; Paolini, R.; Ulpiani, G.; Garshasbi, S.; Fiorito, F. On the energy impact of urban heat island in Sydney: Climate and energy potential of mitigation technologies. *Energy Build.* **2018**, *166*, 154–164. [[CrossRef](#)]
- Santamouris, M.; Haddad, S.; Fiorito, F.; Osmond, P.; Ding, L.; Prasad, D.; Zhai, X.; Wang, R. Urban heat island and overheating characteristics in Sydney, Australia. An analysis of multiyear measurements. *Sustainability* **2017**, *9*, 712. [[CrossRef](#)]
- Yun, G.Y.; Ngarambe, J.; Duhirwe, P.N.; Ulpiani, G.; Paolini, R.; Haddad, S.; Vasilakopoulou, K.; Santamouris, M. Predicting the magnitude and the characteristics of the urban heat island in coastal cities in the proximity of desert landforms. The case of Sydney. *Sci. Total Environ.* **2019**, *709*, 136068. [[CrossRef](#)] [[PubMed](#)]
- Bartasaghi-Koc, C.; Osmond, P.; Peters, A. Quantifying the seasonal cooling capacity of ‘green infrastructure types’ (GITs): An approach to assess and mitigate surface urban heat island in Sydney, Australia. *Landsc. Urban Plan.* **2020**, *203*, 103893. [[CrossRef](#)]
- Khan, H.S.; Santamouris, M.; Paolini, R.; Caccetta, P.; Kassomenos, P. Analyzing the local and climatic conditions affecting the urban overheating magnitude during the Heatwaves (HWs) in a coastal city: A case study of the greater Sydney region. *Sci. Total Environ.* **2021**, *755*, 142515. [[CrossRef](#)] [[PubMed](#)]
- Khan, H.S.; Santamouris, M.; Kassomenos, P.; Paolini, R.; Caccetta, P.; Petrou, I. Spatiotemporal variation in urban overheating magnitude and its association with synoptic air-masses in a coastal city. *Sci. Rep.* **2021**, *11*, 6762. [[CrossRef](#)] [[PubMed](#)]
- Akbari, H.; Cartalis, C.; Kolokotsa, D.; Muscio, A.; Pisello, A.L.; Rossi, F.; Santamouris, M.; Synnefa, A.; Wong, N.H.; Zinzi, M. Local climate change and urban heat island mitigation techniques—The state of the art. *J. Civ. Eng. Manag.* **2015**, *22*, 1–16. [[CrossRef](#)]
- Vuckovic, M.; Maleki, A.; Mahdavi, A. Strategies for development and improvement of the urban fabric: A Vienna case study. *Climate* **2018**, *6*, 7. [[CrossRef](#)]
- Manoli, G.; Fatichi, S.; Schläpfer, M.; Yu, K.; Crowther, T.W.; Meili, N.; Burlando, P.; Katul, G.G.; Bou-Zeid, E. Magnitude of urban heat islands largely explained by climate and population. *Nature* **2019**, *573*, 55–60. [[CrossRef](#)]

19. Lin, P.; Lau, S.S.Y.; Qin, H.; Gou, Z. Effects of urban planning indicators on urban heat island: A case study of pocket parks in high-rise high-density environment. *Landsc. Urban Plan.* **2017**, *168*, 48–60. [[CrossRef](#)]
20. Morakinyo, T.E.; Lam, Y.F. Simulation study on the impact of tree-configuration, planting pattern and wind condition on street-canyon's micro-climate and thermal comfort. *Build. Environ.* **2016**, *103*, 262–275. [[CrossRef](#)]
21. Hien, W.N.; Yok, T.P.; Yu, C. Study of thermal performance of extensive rooftop greenery systems in the tropical climate. *Build. Environ.* **2007**, *42*, 25–54. [[CrossRef](#)]
22. Lin, Y.; Wang, Z.; Jim, C.Y.; Li, J.; Deng, J.; Liu, J. Water as an urban heat sink: Blue infrastructure alleviates urban heat island effect in mega-city agglomeration. *J. Clean. Prod.* **2020**, *262*, 121411. [[CrossRef](#)]
23. Fahed, J.; Kinab, E.; Ginestet, S.; Adolphe, L. Impact of urban heat island mitigation measures on microclimate and pedestrian comfort in a dense urban district of Lebanon. *Sustain. Cities Soc.* **2020**, *61*, 102375. [[CrossRef](#)]
24. Santamouris, M.; Paolini, R.; Haddad, S.; Synnefa, A.; Garshasbi, S.; Hatvani-Kovacs, G.; Gobakis, K.; Yenneti, K.; Vasilakopoulou, K.; Feng, J. Heat mitigation technologies can improve sustainability in cities. An holistic experimental and numerical impact assessment of urban overheating and related heat mitigation strategies on energy consumption, indoor comfort, vulnerability and heat-related mortality and morbidity in cities. *Energy Build.* **2020**, *217*, 110002. [[CrossRef](#)]
25. Santamouris, M.; Yun, G.Y. Recent development and research priorities on cool and super cool materials to mitigate urban heat island. *Renew. Energy* **2020**, *161*, 792–807. [[CrossRef](#)]
26. Gao, K.; Santamouris, M.; Feng, J. On the cooling potential of irrigation to mitigate urban heat island. *Sci. Total Environ.* **2020**, *740*, 139754. [[CrossRef](#)] [[PubMed](#)]
27. Kolokotsa, D.; Lilli, A.A.; Lilli, M.A.; Nikolaidis, N.P. On the impact of nature-based solutions on citizens' health & well being. *Energy Build.* **2020**, *229*, 110527. [[CrossRef](#)]
28. Loeffler, R.; Österreicher, D.; Stoglehner, G. The energy implications of urban morphology from an urban planning perspective—A case study for a new urban development area in the city of Vienna. *Energy Build.* **2021**, *252*, 111453. [[CrossRef](#)]
29. Wang, Y.; Ni, Z.; Hu, M.; Chen, S.; Xia, B. A practical approach of urban green infrastructure planning to mitigate urban overheating: A case study of Guangzhou. *J. Clean. Prod.* **2021**, *287*, 124995. [[CrossRef](#)]
30. Vallati, A.; Mauri, L.; Colucci, C.; Ocloñ, P. Effects of radiative exchange in an urban canyon on building surfaces' loads and temperatures. *Energy Build.* **2017**, *149*, 260–271. [[CrossRef](#)]
31. Lin, P.; Gou, Z.; Lau, S.S.-Y.; Qin, H. The Impact of urban design descriptors on outdoor thermal environment: A literature review. *Energies* **2017**, *10*, 2151. [[CrossRef](#)]
32. Norton, B.A.; Coutts, A.M.; Livesley, S.J.; Harris, R.J.; Hunter, A.M.; Williams, N.S.G. Planning for cooler cities: A framework to prioritise green infrastructure to mitigate high temperatures in urban landscapes. *Landsc. Urban Plan.* **2015**, *134*, 127–138. [[CrossRef](#)]
33. Lindholm, O.; Rehman, H.U.; Reda, F. Positioning positive energy districts in european cities. *Buildings* **2021**, *11*, 19. [[CrossRef](#)]
34. de Dear, R.; Kim, J.; Parkinson, T. Residential adaptive comfort in a humid subtropical climate—Sydney Australia. *Energy Build.* **2018**, *158*, 1296–1305. [[CrossRef](#)]
35. Stewart, I.D.; Oke, T.R. Local climate zones for urban temperature studies. *Bull. Am. Meteorol. Soc.* **2012**, *93*, 1879–1900. [[CrossRef](#)]
36. Garshasbi, S.; Haddad, S.; Paolini, R.; Santamouris, M.; Papangelis, G.; Dandou, A.; Methymaki, G.; Portalakis, P.; Tombrou, M. Urban mitigation and building adaptation to minimize the future cooling energy needs. *Sol. Energy* **2020**, *204*, 708–719. [[CrossRef](#)]
37. Morakinyo, T.E.; Lau, K.K.-L.; Ren, C.; Ng, E. Performance of Hong Kong's common trees species for outdoor temperature regulation, thermal comfort and energy saving. *Build. Environ.* **2018**, *137*, 157–170. [[CrossRef](#)]
38. Bruse, M. Modelling and strategies for improved urban climates. In Proceedings of the Biometeorology and Urban Climatology at the Turn of the Millennium, Sydney, NSW, Australia, 8–12 November 1999.
39. Masson-Delmotte, V.; Zhai, P.; Pörtner, H.-O.; Roberts, D.; Skea, J.; Shukla, P.R.; Pirani, A.; Moufouma-Okia, W.; Péan, C.; Pidcock, R.; et al. (Eds.) *IPCC, 2018: Global Warming of 1.5°C*; IPCC: Geneva, Switzerland, 2018.
40. Pachauri, R.K.; Allen, M.R.; Barros, V.R.; Broome, J.; Cramer, W.; Christ, R.; Church, J.A.; Clarke, L.; Dahe, Q.; Dasgupta, P.; et al. Contribution of Working Groups I, II and III to the Fifth Assessment Report of the Intergovernmental Panel on Climate Change. In *Climate Change 2014: Synthesis Report*; Pachauri, R., Meyer, L., Eds.; IPCC: Geneva, Switzerland, 2014; p. 151. ISBN 978-92-9169-143-2.
41. Cilek, M.U.; Cilek, A. Analyses of land surface temperature (LST) variability among local climate zones (LCZs) comparing Landsat-8 and ENVI-met model data. *Sustain. Cities Soc.* **2021**, *69*, 102877. [[CrossRef](#)]
42. Liu, Z.; Cheng, W.; Jim, C.; Morakinyo, T.E.; Shi, Y.; Ng, E. Heat mitigation benefits of urban green and blue infrastructures: A systematic review of modeling techniques, validation and scenario simulation in ENVI-met V4. *Build. Environ.* **2021**, *200*, 107939. [[CrossRef](#)]
43. López-Cabeza, V.; Galán-Marín, C.; Rivera-Gómez, C.; Fernández, J.R. Courtyard microclimate ENVI-met outputs deviation from the experimental data. *Build. Environ.* **2018**, *144*, 129–141. [[CrossRef](#)]
44. Forouzandeh, A. Prediction of surface temperature of building surrounding envelopes using holistic microclimate ENVI-met model. *Sustain. Cities Soc.* **2021**, *70*, 102878. [[CrossRef](#)]
45. Oke, T.R. *Boundary Layer Climates*, 2nd ed.; Methuen & Co. Ltd.: London, UK, 1987; ISBN 9780415043199.